Sixth International Symposium on Turbulence and Shear Flow Phenomena
Seoul, Korea, 22-24 June 2009

LARGE-EDDY SIMULATION OF A LAMINAR SEPARATION BUBBLE: THE SMAGORINSKY AND DYNAMIC MODELS

S. Sarkar
Department of Mechanical Engineering,
Indian Institute of Technology Kanpur, India
subra@iitk.ac.in

N. K. Singh
Department of Mechanical Engineering,
Indian Institute of Technology Kanpur, India
nirks@iitk.ac.in

ABSTRACT

The principal objective of the present simulation is to find the ability of Large-eddy simulation (LES) to resolve the transition mechanism of a laminar separation bubble apart from making a comparative assessment of subgrid-scales (SGS) models. The Smagorinsky model modified by the low-Reynolds number correction of Voke (1996) and the dynamic model are used to account for the non-resolvable subgrid stresses. Two values of the Smagorinsky constant C_s have been tested. Results from the dynamic model are closer to the DNS data compared to those from the Smagorinsky model. The simulation shows that no significant growth of fluctuations is observed in the first 27 percent of bubble length. Three-dimensional motion and non-linear interactions leading to break down to turbulence occur in the second half of the mean bubble length. The simulation also illustrates that the transition process is characterized by break down of longitudinal streaks, which appear via vortex stretching mechanism. The near wall characteristics develop far downstream indicating a very slow relaxation towards an equilibrium turbulent boundary layer.

INTRODUCTION

When a flow at relatively low Reynolds Number encounters an adverse pressure gradient, it may separate from the solid surface. The boundary layer leaves the surface approximately in a tangential direction forming a wedge shaped separated region. The separated but still laminar flow is highly sensitive to the external disturbances, which cause the flow to undergo transition. The transition region is located at the outer boundary of the separated shear layer; the thickness of the shear layer grows rapidly and it may finally reattach to the solid surface as a turbulent layer. The point where the laminar boundary layer separates from the solid surface is known as the *point of separation* and the point where the turbulent boundary layer reattaches to the surface again is known as *reattachment point*. The volume occupied by the regions of separated laminar flow and the turbulent flow is known as *laminar separation bubble.* The structure of a time averaged laminar separation bubble, given by Horton (1968) is reproduced in Fig. 1.

The existence of a laminar separation bubble was first recognized by Jones (1934). The work was further carried out by Gault (1957). The most notable advancement in the understanding of bubble structure and behaviour came with the work of Gaster (1968). He investigated a large number of bubbles produced on a flat surface. A numerical study of 2-D laminar separation bubble using N-S equations was done by Briley (1971). Pauley and co-workers (1990, 1993) first pointed out the unsteady nature of laminar separation. Pauley's analyses were 2-D and the effects of small-scale turbulence were completely neglected. Alam and Sandham (2000) performed a direct numerical simulation (DNS) of the incompressible N-S equations to study flows where laminar boundary-layer separation is followed by turbulent reattachment. In a recent work of Sarkar and Voke (2006), the physical mechanism of transition of an inflectional boundary layer over the suction surface of a highly cambered low-pressure turbine blade under the influence of periodically passing wakes was studied in detail

The appearance of a laminar separation bubble is very common in case of low Reynolds number flows on wings and blades. The performance of almost all aircraft is influenced by the appearance of the laminar separation bubble. A separation bubble is often formed on the suction surface of a LP turbine. The boundary layer development depends on the growth and breakdown of this bubble. The flow transition over the separation bubble is complex and has been investigated by several researchers. DNS carried out by Spalart and Strelets (1997) and Alam and Sandham (2000) explain the transition mechanism apart from the flow structures. However, despite the incredible computing power available today, the cost of DNS is prohibitive and LES may be an alternative.

The present study is an effort to explore the viability of simulating the laminar separation bubble using LES. Simulations have been performed using the Smagorinsky model modified by the low-Reynolds number correction of Voke (1996) and the dynamic model. Two values of the Smagorinsky constant C_s have been tested. Results obtained from the simulations are compared to the available DNS data.

METHODS

Numerical procedures

In the present study, we perform LES of incompressible flow. The filtered mass and momentum equations can be expressed as,

$$\frac{\partial \overline{u}_j}{\partial x_j} = 0 \tag{1}$$

$$\frac{\partial \overline{u}_i}{\partial t} + \frac{\partial}{\partial x_j}\left(\overline{u}_j \overline{u}_i\right) = -\frac{1}{\rho}\frac{\partial \overline{P}}{\partial x_i} + \frac{1}{\mathrm{Re}_{\delta^*_{in}}}\nabla^2 \overline{u}_i - \frac{\partial \tau_{ij}}{\partial x_j} \tag{2}$$

Where, $\overline{u}$ denotes the filtered velocity field and $\tau_{ij} = \overline{u_i u_j} - \overline{u}_i \overline{u}_j$ denotes residual stress tensor (also known as subgrid scale stress, SGS). The above equations have been made dimensionless using free stream velocity U_∞ and the boundary layer displacement thickness at inlet δ^*_{in}. The resulting Reynolds number is $\mathrm{Re}_{\delta^*_{in}} = U_\infty \delta^*_{in} / \nu$, ν being the kinematic viscosity. The Smagorinsky model modified by the low-Reynolds number correction of Voke (1996) and the dynamic model are used to account for the non-resolvable subgrid stresses. The Smagorinsky model is based on local large-scale quantities and predicts nonzero residual stresses even in the laminar region. It is incapable of predicting the reverse cascade regions and overestimates the subgrid-scale dissipation. Part of the limitation has been overcome by using the low-Reynolds number model of Voke (1996), which is derived following the dissipation spectrum and is expected to simulate the transitional flow. The dynamic SGS model proposed by Germano et al. (1991) and modified by Lilly (1992) is used here, where the model coefficient is dynamically calculated instead of input a priori.

In the present simulations the momentum advancement is explicit using the second-order Adams-Bashforth scheme except for the pressure term which is solved by a standard Projection method. Pressure Poisson equation is discrete Fourier transformed in one dimension (in which periodicity of the flow and so uniformity of the geometry is imposed) and solved using the Bi-Conjugate Gradient method. The spatial discretization is second-order accurate using a symmetry preserving central difference scheme, which is widely used in LES owing to its non-dissipative and conservative properties.

Computational details

The Schematic view of the computational domain is shown in Fig. 2. The length scales are normalized with respect to inlet boundary layer displacement thickness (δ^*_{in}), and the velocity scale with respect to inlet free stream velocity (U_∞). The box length and the number of grid points used for the simulation are shown in the tabular form in Table 1. A uniform grid spacing is used in the streamwise (x) and spanwise (z) directions, whereas, a slow stretching is used in the wall normal direction (y). The flow field is initiated by specifying a Blasius velocity profile to the streamwise velocity component and the wall normal velocity is set to zero. At the outlet, a convective boundary condition has been used. At the lower boundary i.e. in the solid wall a no-slip condition is applied. In the present simulation, a disturbance strip is provided at the wall and upstream of separation to trigger the transition. The disturbance is specified by a function to the normal velocity following the work of Alam and Sandham (2000)

$$v'(x, z, t) = a_f \exp[-b_f (x-c_f)^2] \sin(\omega t) \sin(\beta z) \tag{3}$$

where the constants a_f, b_f and c_f control the streamwise variation of the perturbation. ω is the frequency of the disturbance and β, the span wise wave number.

The simulation is performed on a flat plate and thus an adverse pressure gradient is created by a suitable upper boundary condition for flow to separate. The normal velocity component at the upper boundary has been specified by a Gaussian suction profile given by the following expression,

$$S(x) = a_s \exp[-b_s (x-c_s)^2] \tag{4}$$

where the constants a_s, b_s and c_s control the size, shape and location of the suction profile. The values of the constants can be found in Alam and Sandham (2000). A periodic boundary condition is applied to the homogeneous spanwise direction.

The boundary-layer is allowed to grow over the flat plate with imposed boundary conditions. Solution is advanced with a time step of $\Delta t = 0.02$ in non-dimensional units that needs 10000 iterations for a flow pass. We allowed seven flow passes with wall disturbances to develop the turbulences and the separation bubble. Statistics were taken for further ten flow passes. All data generated are analyzed by time-averaging as well as through the study of instantaneous dynamics and spectral analysis.

A grid-resolution test is carried out using four levels of mesh, viz. $160 \times 64 \times 32$, $200 \times 64 \times 32$, $200 \times 64 \times 64$ and $260 \times 64 \times 64$ grid points in the x, y and z directions. Variation of mean skin friction coefficient (C_f) for different grids is depicted in Fig. 3, while profiles of mean streamwise velocity along with the turbulent kinetic energy (TKE) are shown in Fig. 4. It can be seen from Fig. 3 that bubble length does not change significantly on further refinement of grid from $200 \times 64 \times 64$. Fig. 4 further corroborates this fact. It shows that values of mean streamwise velocity change little on further refinement but TKE values do change a bit. Hence, a grid of 200x64x64 points is chosen for the calculations. The near wall resolution at x = 170, where an attached turbulent layer

appears, is $\Delta x^+ = 20$, $\Delta y^+ = 1.0$ and $\Delta z^+ = 10$. Here, the Reynolds number based on δ^*_{in} and U_∞ ($Re_{\delta^*_{in}}$) is 500.

RESULTS AND DISCUSSION

The aim of the paper, as mentioned earlier, is to study the characteristics of laminar separation bubble subjected to wall disturbances through LES using Smagorinsky and dynamic models. Results obtained from these models are compared with the DNS data available in the literature to evaluate the suitability of these models for separating and reattaching flows.

Mean skin friction coefficient

Fig. 5 shows the variation of mean skin friction coefficient for different test cases and compared with the DNS. The skin friction coefficient is given by $C_f = 2\tau_w / \rho U_e^2$ where τ_w is the wall shear stress & U_e is the local free-stream velocity. The potential flow is locally distorted in the vicinity of the bubble that does not allow having a unique value of free-stream velocity. Hence the skin friction coefficient is normalized by a local free-stream velocity (U_e) that was defined by integration of spanwise vorticity following Spalart & Strelets (1997)

$$U_e(x,y) = -\int_0^y \omega_z dy$$

The plot of the mean skin friction gives information about the mean bubble length. The separation and reattachment points of the mean flow are located by the zero crossing of the skin friction plots, Fig 5. In the skin friction distribution, the initial flat portion after the separation point corresponds to the dead air region of the bubble, whereas, the reverse flow vortex region is associated with a much larger negative skin friction. When compared with the corresponding data of Alam and Sandham (2000), it is evident that results from the dynamic model are closer to the DNS.

Mean flow structures

A few important variables which are used to describe the mean flow features are Reynolds numbers based on the boundary layer momentum thickness at separation (Re_{θ_s}) and transition length (Re_{lt}). The length of transition is taken here as the distance from separation point to the point of minimum skin friction. The length of separation bubble is also calculated from C_f distributions for both the Smagorinsky and Dynamic models. The values of these parameters have been given in the Table 2 and Table 3 and compared with the corresponding values obtained from the DNS (Alam and Sandham, 2000). A comparison of the tabulated values clearly shows that the Smagorinsky model with $C_s = 0.17$ gives the worst results in general while the dynamic model provides the best. Fig. 7 shows the streamwise velocity contours for the dynamic model illustrating the shape of the bubble. The dead-air region and the reverse flow vortex are also indicated. The pictorial views of the bubbles from both the models are more or less the same but the similarity of the view from the dynamic model with that obtained from DNS is striking.

Fig. 8 shows the mean streamwise velocity component and the r.m.s. of streamwise and wall-normal velocity fluctuations. The horizontal axis of the Fig. 8 is arbitrarily chosen to represent the variation in magnitude of the variables with respect to the change in position along the streamwise direction. The boundary layer over the flat plate develops against an adverse pressure gradient that cause the boundary layer to separate from the solid surface near x=22 which is reflected by an inflectional velocity profile. It also illustrates the growth of the shear layer, separation bubble with a backflow region and the reattachment point near x=43. After the reattachment, the separated shear layer relaxes downstream slowly towards an equilibrium turbulent boundary layer. Fig. 8 also indicates the evolution of turbulence after the separation. Though the perturbations start growing just downstream of separation, the initial growth rate, particularly for v', is slow and after x=39 the growth rate is appreciable. This location coincides with the location of minimum C_f. Thus it can be inferred that the generation of turbulence occurs mainly in the reverse flow region and not in the dead air region. After the reattachment, it takes several bubble lengths downstream to develop the near wall turbulent characteristics.

Transition and reattachment

The instantaneous flow field is very revealing and can be used to explain transition mechanism over the separation bubble, associated flow structures and their breakdown to turbulence after reattachment.

Fig. 9(a) shows contours of streamwise velocity in x-y plane (side view) for z=30.0. The darkest gray-scale represents the separation region. It also illustrates thickening of shear layer over the bubble and the rollup of shear layer in the outer region illustrating that instability of shear layer occurs via Kelvin-Helmholtz mechanism. This process creates large-scale vortices that may retain their structures far downstream. Thus, near the reattachment, the boundary layer is characterized by predominant outer layer activities that may generate high turbulence in the outer region. Furthermore, referring to Fig. 6 depicting TKE profiles at different locations, the TKE is seen to rapidly increase over the rear half of the bubble. The peaks also shift away from the wall illustrating that turbulence is dominant in the outer part of the layer. Characteristics of near-wall turbulence develop only several bubble lengths downstream.

Fig. 9 (b) shows the top view (x-z plane) of streamwise velocity contours for a wall normal location y=0.05. The top-view illustrates that the initial flow-field is two-dimensional and the boundary layer separates as laminar. The perturbations appear to grow and the flow ceases to be two-dimensional downstream of x=25. Three-dimensionality appears downstream of x=30 and longitudinal streaks, the characteristics of transitional layer, appear near x=39. This location corresponds to the minimum C_f (Fig. 5). The development of these low-speed

streaks near the reattachments regions and their breakdown is also depicted. The top view further confirms that the near wall turbulence develops far downstream of reattachment

Fig. 9(c) shows the cross-sectional views (y-z plane) of streamwise velocity contours for different streamwise locations at the same time. The contours at x = 31.0 exhibit the initial symmetry and two-dimensionality of the flow. The two-dimensionality is seen to be slightly distorted at x=50 and is completely destroyed downstream of x=83 making the flow three-dimensional.

Fig. 10 shows that the value of shape factor (δ^* / θ) at reattachment is 3.3 which is in excellent agreement with Horton's value 3.5. Far downstream the value drops down to approximately 1.5 indicating approach to equilibrium. Fig. 11 shows the non-dimensionalized TKE production in the near wall region. Near the reattachment point, the flow is characterized by high active outer layer and this shifts to the inner layer with generation of turbulence after x=70. Beyond x= 90, collapse of the profiles is striking. They agree with each other and with the data of Kim et al. illustrating a slow approach to the equilibrium turbulent boundary layer.

The contours of Reynolds stresses obtained from LES using the dynamic model are presented in Fig. 12. The imposed disturbances at x=10 are reflected in contours of $\overline{u'u'}$ and $\overline{w'w'}$ upstream of separation. These disturbances decay downstream until the highly unstable separated shear layer is encountered. Here, the Reynolds stresses are amplified reaching the maximum values near the reattachment point. In this region, the shear layer spreads away from the wall while steep gradients of $\overline{u'u'}$ and $\overline{u'v'}$ near the wall appear far downstream, x=100. The distributions of shear stresses along with the magnitude are of levels similar to the DNS (Alam & Sandham, 2000).

In brief, the boundary layer just downstream of reattachment appears very different from an equilibrium turbulent boundary layer and the relaxation is very slow downstream.

CONCLUSIONS

Large eddy simulation of a short laminar bubble has been carried out using Smagorinsky and dynamic models and compared with the DNS results. The present LES with dynamic model produces encouraging results, illustrating transition process over the separation bubble. After the separation, almost no growth of fluctuations is observed in the first 27 percent of bubble length and thereafter the fluctuations increase rapidly. Thus, 3-D motion and non-linear interactions leading to break down to turbulence occur in the second half of the mean bubble length. The simulation also illustrates that the transition process is characterized by break down of longitudinal streaks. Turbulence statistics reflects that the turbulent activities are dominant in the outer layer over the rear half of the bubble and near the reattachment. The near wall characteristics develop far downstream indicating a very slow relaxation towards an equilibrium turbulent boundary layer.

REFERENCES

Alam, M., and Sandham, N. D., 2000, "Direct numerical simulation of 'short' laminar separation bubbles with turbulent reattachment", *Journal of Fluid Mechanics*, Vol. **403**, pp. 223–250.

Briley, W.R., 1971, "Numerical Study of Laminar Separation Bubbles Using the Navier-Stokes Equations", *Journal of Fluid Mechanics*, Vol. **47**, Part 4, pp. 713-736.

Gaster, M., 1968, "Growth of Disturbances in Both Space and Time", *Physics of Fluids*, Vol. **11**, pp.723-727

Gault, D. E., 1957, "A Correlation of Low-speed Airfoil Section Stalling Characteristics with Reynolds Number and Airfoil Geometry", *NACA TN 3963*.

Germano, M., Piomelli, U., Moin, P. and Cabot, W.H., 1991, "A dynamic subgrid-scale eddy viscosity model", *Physics of Fluids A*, Vol. **3**, pp. 1760-65.

Horton, H.P., 1968, *Laminar separation in two and three-dimensional incompressible flow*, PhD Dissertation, University of London.

Jones, B. M., 1934, "Stalling", *Journal of Royal Aeronautical Society*, Vol. **38**, pp. 753–770.

Lilly, D.K., 1992, "A proposed modification of the Germano subgrid-scale closure method", *Physics of Fluids A*, Vol. **4**, pp. 633-35.

Pauley, L. L., Moin, P., and Reynolds, W. C., 1990, "The Structure of Two-dimensional Separation", *Journal of Fluid Mechanics*, Vol. **220**, pp.397-412.

Ripley M. D., and. Pauley, L. L, 1993, "The Unsteady Structure of Two-dimensional Steady Laminar Separation", *Physics of Fluids A*, Vol. **5**(12).

Sarkar, S., and Voke, P. R., 2006, "Large-eddy simulation of unsteady surface pressure over a LP turbine due to interactions of passing wakes and inflexional boundary layer," *ASME Journal of Turbomachinary* , Vol. **128**, pp. 221-231

Spalart, P.R., and Strelets, M.K., 1997, "Direct and Reynolds-averaged numerical simulation of a transitional separation bubble", *11th symp. on Turbulent shear Flows,* Grenoble, France.

Voke, P. R., 1996, "Subgrid-scale modeling at low mesh Reynolds number", *Theoretical and Computational Fluid Dynamics*, Vol. **8**, pp. 131-143.

Table 1: Computational grid and box sizes

Cells	$L_x(\delta^*_{in})$	$L_y(\delta^*_{in})$	$L_z(\delta^*_{in})$
$200\times64\times64$	200	10	30

Table 2: points of separation and reattachment for different simulations

Case	Point of Separation	Point of Reattachment
Dynamic model	22	43
Smagorinsky, C_S=0.1	22	45
Smagorinsky,C_S=0.17	23	51

Table 3: Data related to mean bubble shape

Case	Re_{θ_s}	l_b/δ^*_{in}	θ_s/δ^*_{in}	Re_{lt}
DNS,Alam-Sandham	246	16.4	0.49	6667
Dynamic model	210	21	0.42	8500
Smagorinsky, C_S =0.1	213	23	0.43	9500
Smagorinsky,C_S =0.17	255	28	0.51	11000

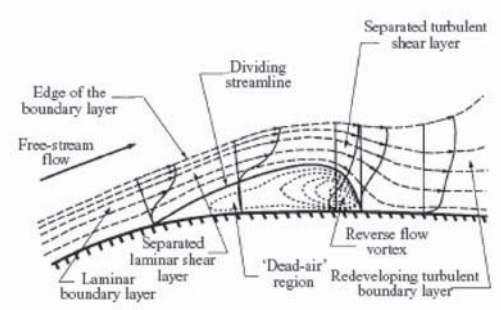

Figure 1: Classical structure of a short laminar separation bubble

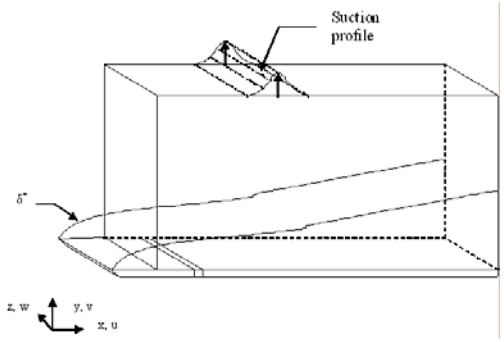

Figure 2: Schematic drawing of the computational domain

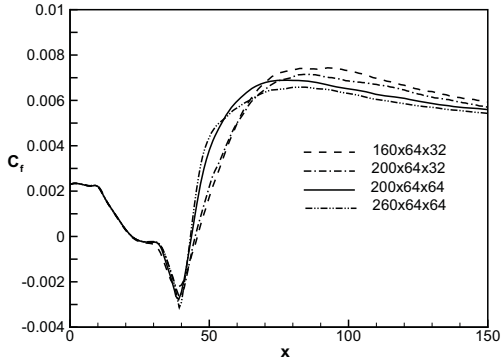

Figure 3. Comparison of skin friction variation for different grids.

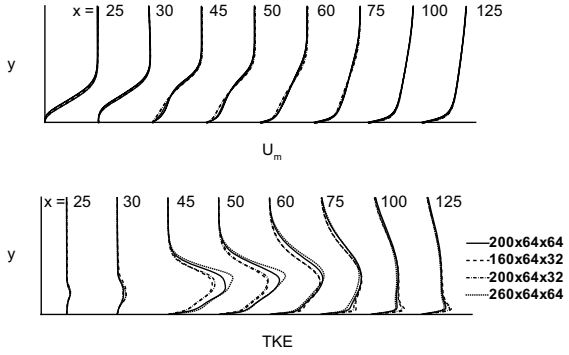

Figure 4: Profiles of mean streamwise velocity and TKE at indicated locations for different grids

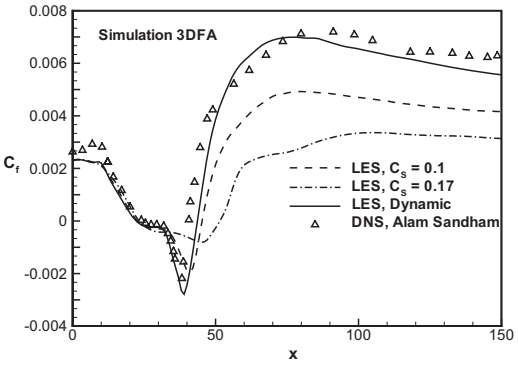

Figure 5. Comparison of skin friction variation for SGS models with DNS of Alam and Sandham (2000).

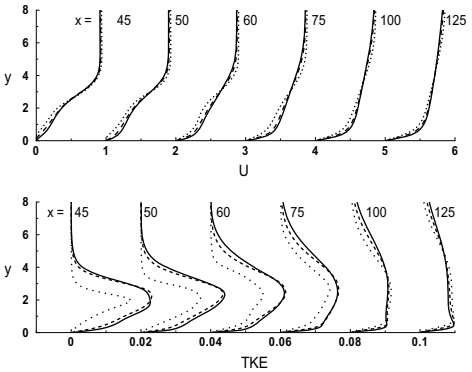

Figure 6. (a) Mean streamwise velocity and (b) TKE profiles at different locations: solid lines for the Dynamic model, dashed lines for the Smagorinsky model with C_s =0.1 and dotted lines for C_s=0.17.

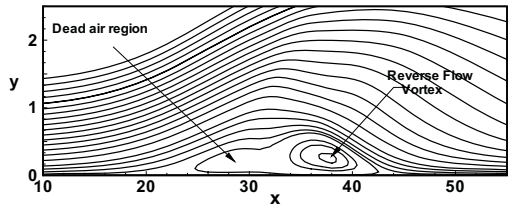

Figure 7 Streamwise velocity contours of the laminar separation bubble.

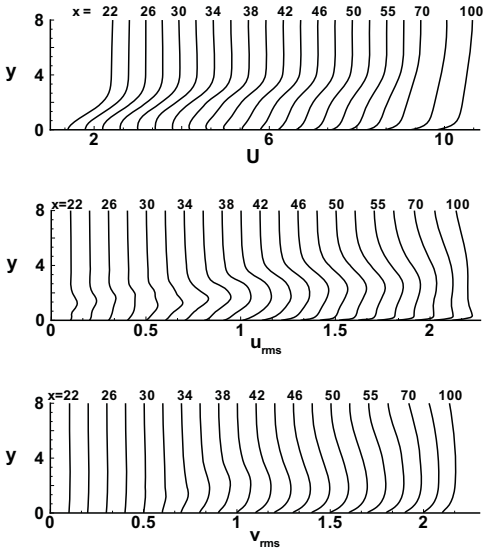

Figure 8. Profiles of mean streamwise velocity, rms streamwise velocity fluctuation and rms wall-normal velocity fluctuation at different locations.

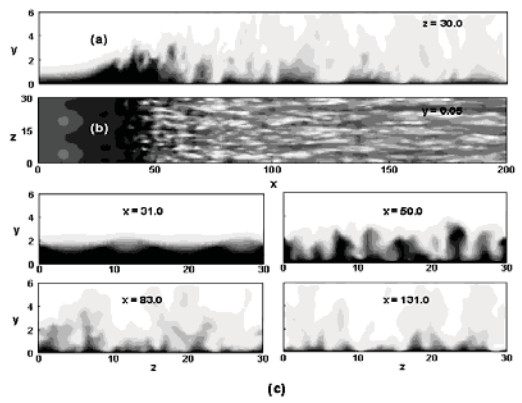

Figure 9. Instantaneous contours of streamwise velocity of a bubble with turbulent reattachment. Maximum level is 0.98, minimum level is -0.13 and the darkest colour shows reversed flow. (a) (x,y)-plane at z = 30.0, (b) (x,z)-plane at y = 0.05, (c) (y,z)- plane at x = 31.0, 50.0, 83.0 and 131.0.

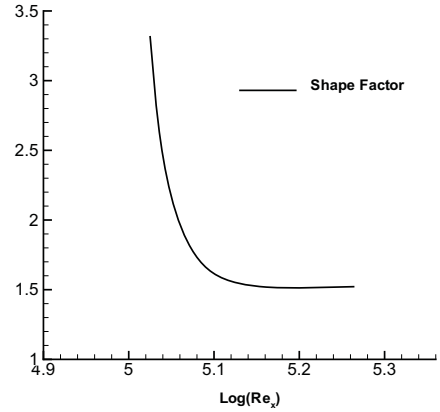

Figure 10. Shape factor after reattachment .

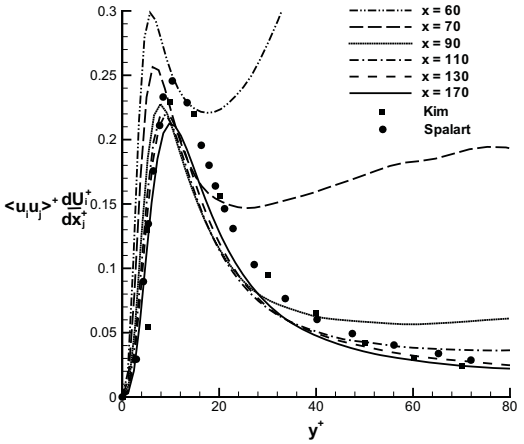

Figure 11. Time-averaged non-dimensional TKE production near the wall.

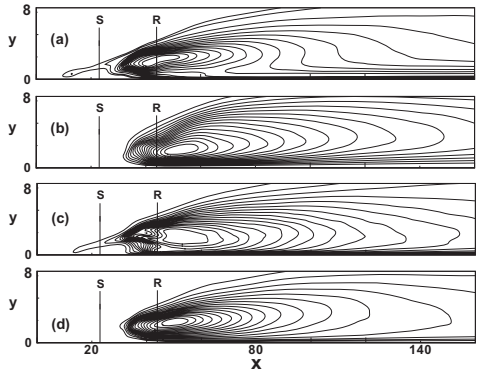

Figure 12. Contours of fluctuation statistics: (a) $\overline{u'u'}$, (b) $\overline{v'v'}$, (c) $\overline{w'w'}$ and (d) $\overline{u'v'}$. Maximum contour levels are 0.0282, 0.0095, 0.0113 and 5.21×10^{-4} respectively.